Available online at www.sciencedirect.com

ScienceDirect

journal homepage: www.elsevier.com/locate/he

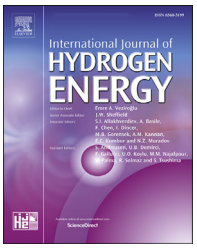

Hydrogen-diesel dual-fuel direct-injection (H2DDI) combustion under compression-ignition engine conditions

Patrick Rorimpandey [a], *Ho Lung Yip* [a], *Aleš Srna* [b], *Guanxiong Zhai* [a], *Armin Wehrfritz* [c], *Sanghoon Kook* [a], *Evatt R. Hawkes* [a], *Qing Nian Chan* [a,*]

[a] *School of Mechanical and Manufacturing Engineering, The University of New South Wales, NSW, 2052, Australia*
[b] *Combustion Research Facility, Sandia National Laboratories, Livermore, CA, 94551, USA*
[c] *Mechanical Engineering, University of Turku, Turun Yliopisto, FI-20014, Finland*

ARTICLE INFO

Article history:
Received 9 June 2022
Received in revised form
20 September 2022
Accepted 25 September 2022
Available online xxx

Keywords:
Hydrogen
Dual fuel
Direct injection
Compression-ignition engine

ABSTRACT

This study investigates the ignition and combustion characteristics of interacting diesel-pilot and hydrogen (H_2) jets under simulated compression-ignition engine conditions. Two converging single-hole injectors were used to inject H_2 and diesel-pilot jets into an optically accessible constant-volume combustion chamber (CVCC). The parameters varied include fuel injection sequence, timing between injections, and ambient temperature (780–890 K). The results indicate that when diesel-pilot is injected before H_2, with increasing time separation, the burnt diesel products mix and cool down, requiring longer jet-jet interaction to ignite the H_2 jet. When H_2 is injected before diesel-pilot, the H_2-air mixing amount prior to pilot-fuel igniting impacts the combustion spreading through the H_2 jet. If ignition of the H_2 jet occurs beyond its end-of-injection (EOI), the H_2 mixture zone where the pilot-diesel interacts with becomes too lean for combustion. At lower ambient temperatures, the combustion variability increases, attributed to the diesel-pilot lean out.

Introduction

Hydrogen (H_2) is considered a potential energy carrier in transportation powertrains because of its carbon-neutral and renewable potential [1–3]. As a fuel in internal combustion engines (ICE), the wide flammability limit (4–76 vol% in air) and high laminar flame speed of H_2 (1.85 m/s in air [a,c,d])[1] result in a short combustion duration even under very lean operation, which increases the thermal efficiency [1,4,5]. Nonetheless, the low volumetric density and minimum ignition energy of H_2 pose challenges for traditional H_2 ICE applications with port fuel injection. Due to the low volumetric energy content (10.7 MJ/m^3 [a,b]), the engine volumetric efficiency is reduced. Despite a high autoignition temperature (858 K [6]), the low minimum ignition energy of H_2 (0.02 mJ [a,d]) [4,6] increases the pre-ignition tendency of H_2 by hot spots or residues within the engine chamber, leading to a loss of combustion phasing control, knocking and possible mechanical engine failure [1,7]. The short quenching distance of H_2

* *Corresponding author.*
E-mail address: qing.chan@unsw.edu.au (Q.N. Chan).

[1] [a] at 1 bar, [b] at 273 K, [c] at 298 K and [d] at stoichiometry.

https://doi.org/10.1016/j.ijhydene.2022.09.241

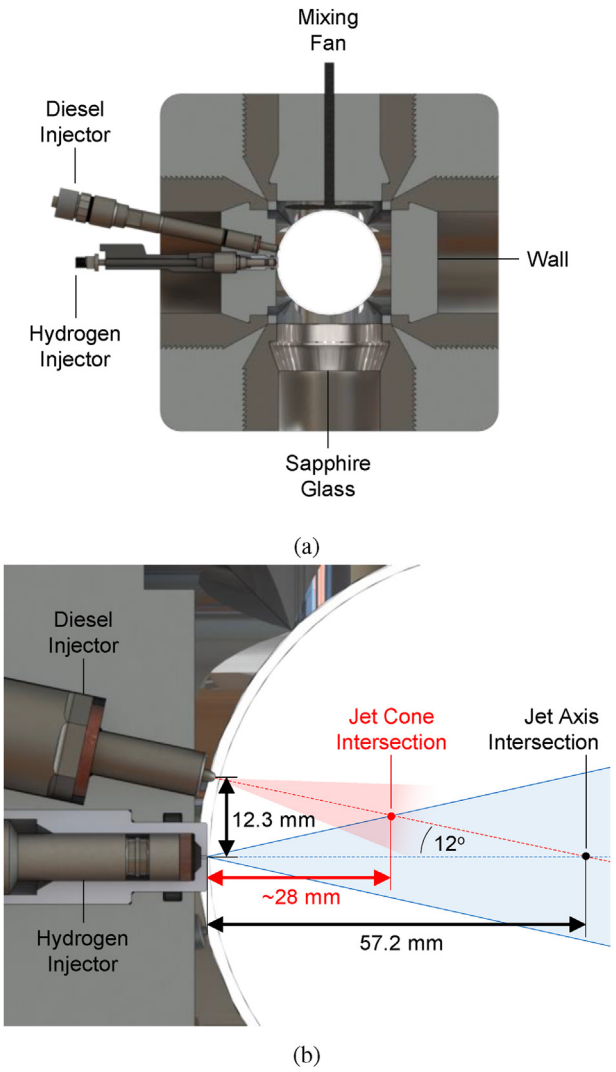

Fig. 1 – (a) Cross-section schematic of the constant-volume combustion chamber. (b) Detailed view of the H_2 and diesel injector layouts, showing symbolic H_2 (blue) and *n*-heptane jet cones (red), with the points of jet axis and cone intersection. (For interpretation of the references to colour in this figure legend, the reader is referred to the Web version of this article.)

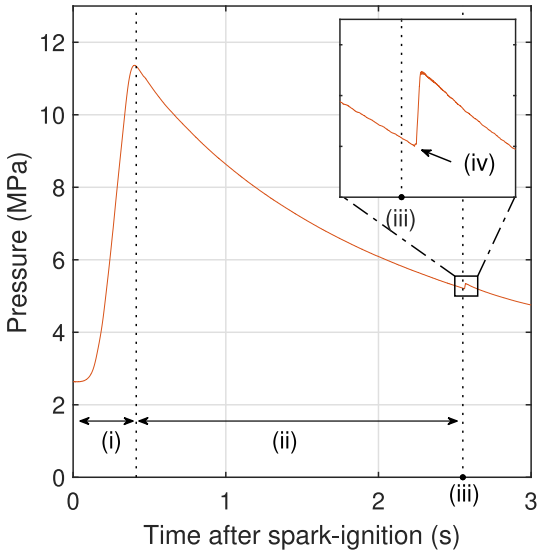

Fig. 2 – Sample CVCC pressure trace data during an experiment run. Starting at spark ignition, it highlights the following four key events: (i) premixed ambient gas combustion, (ii) cool-down period, (iii) start of fuel injection and (iv) fuel ignition.

Table 1 – Summary of the experimental conditions. Bold values are the reference conditions.

CVCC Ambient Conditions	
Wall temperature (K)	403
Ambient O_2 concentration (vol%)	21
Ambient gas density (kg/m^3)	23.8
Ambient gas pressure (MPa)	**5.20**, 4.60, 4.45
Ambient core gas temperature (K)	**890**, 820, 780

(0.64 mm [a,c,d]), combined with its high laminar flame speed, implies an increased backfiring risk into the intake manifold, and higher temperature gradients near the cylinder wall that increases heat loss and engine oil consumption.

Various in-cylinder mixture preparation and ignition processes have been studied previously, and direct injection (DI) of H_2 was shown to alleviate backfiring, pre-ignition, and volumetric efficiency loss challenges associated with port and manifold injection approaches [1,4,8]. The requirement of an additional ignition source was noted since the high H_2 auto-ignition temperature requires intake-air preheating or impractical compression ratio (CR) of >26–42 for reliable compression ignition (CI) [9,10]. Different ignition options include spark discharge ignition [11–13], hot surface [14,15], or pilot-fuel ignition (dual-fuel) [16–18,54]. This study focuses on the dual-fuel combustion approach, which involves creating a high-temperature environment via diesel-fuel combustion to ignite the H_2 main fuel. The dual-fuel approach was successfully commercialized for natural-gas engines, where exceptional combustion stability was demonstrated, aside from the operational flexibility as such engines can operate on diesel fuel only if needed [19–21]. Some dual-fuel engines operate with early main fuel injection to create a homogeneous or moderately stratified gaseous fuel mixture ignited by a pilot fuel injection near TDC, with flame propagation as the dominant combustion mechanism [22]. Such engines typically exhibit good efficiency and low pilot-fuel consumption [23,24], but do not entirely eliminate the pre-ignition issues. Late high-pressure main-fuel injection is a more robust approach for dual-fuel H_2 engine applications. In this concept, the main-fuel and pilot-fuel are injected near the TDC, and diffusion combustion is the dominant fuel conversion process [20].

The H_2-diesel dual-fuel direct-injection (H2DDI) mode is a relatively novel approach with limited experimental or numerical studies. However, previous studies utilising natural gas as the main fuel identified various factors that will likely affect the ignition and combustion processes of H2DDI. The relative orientation between the injectors—which can be categorized as diverging (the injectors are directed away from

Please cite this article as: Rorimpandey P et al., Hydrogen-diesel dual-fuel direct-injection (H2DDI) combustion under compression-ignition engine conditions, International Journal of Hydrogen Energy, https://doi.org/10.1016/j.ijhydene.2022.09.241

Table 2 – Summary of injection conditions and fuel properties [4,16,37].

Fuel Injection Conditions		
Fuel	*n*-heptane	H_2
Nozzle diameter (mm)	0.105	0.58
Fuel reservoir pressure (MPa)	70	20
Electronic injection command duration (ms)	0.4	3.0
Hydraulic injection duration (ms)	0.7	3.3
Mass injected (mg)	0.99	5.28
Low. heat. value [38] (MJ/kg)	43.2	120.0
Energy (J)	43.2	633.6
Total energy (J)	676.8	
Energy share (%)	6.4	93.6
Research octane number (RON)	0	130
Cetane number	56	–
Density at 293.15 K (kg/m^3)	680	0.09
Auto-ignition temperature (K)	493.15	856

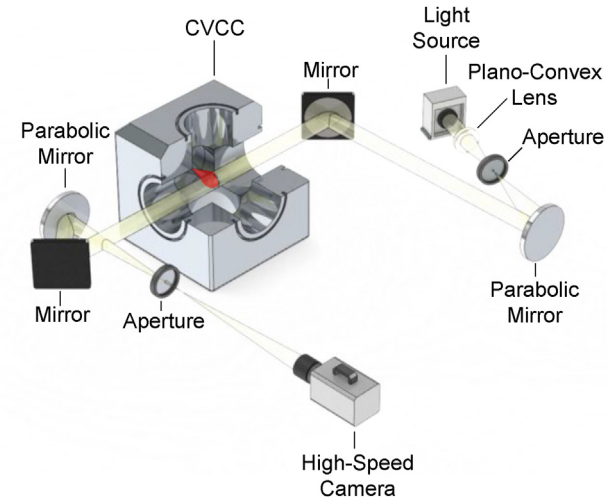

Fig. 3 – A schematic of the combustion vessel and the high-speed schlieren imaging optical arrangement. The light path (transparent yellow) from the schlieren imaging light source and a model of the penetrating jet (red) are shown. (For interpretation of the references to colour in this figure legend, the reader is referred to the Web version of this article.)

each other), parallel (the injector axes are aligned) or converging (the injector axes intersect downstream) [25]—can affect fuel interaction and the ensuing combustion process. There are several studies of the effects of jet orientation on the combustion processes. Li et al. [21] reported a statistical correlation between the combustion instabilities of their engine performance tests with the changing spatial interaction between the pilot diesel and natural gas jets that their integrated two-fuel HDPI multi-hole injector produced. More recent studies by Fink et al. [26,27] provided direct visualisation of the dependency of ignition and combustion processes on the spatial jet interaction, which showed improved ignition with converging jet arrangements, especially at low ambient temperature. It is noteworthy that other studies have shown that the pilot-fuel entrainment into the main-fuel jet can quench the pilot-fuel autoignition [26–28].

Previous natural-gas dual-fuel studies also showed the importance of the fuel injection sequence (pilot-fuel or main-fuel injected first, and the associated dwell time) on combustion stability, peak AHRR, and combustion noise. It was demonstrated that the combustion noise and peak apparent heat release rate (AHRR) are reduced when the main-fuel is ignited as early after injection as possible, which occurs when pilot-fuel is injected somewhat before the main injection [20,26,29,30]. This is associated with the minimal degree of main-fuel premixing at the time of ignition by the pilot fuel. At other dwell times, the interaction of main fuel with pilot is delayed (main fuel injected before pilot), or the pilot-fuel burnt gases cool down due to mixing (pilot injected long before main). Both cases delay the main-fuel ignition and increase the AHRR. At more extreme timings, the ignition and combustion become unstable, resulting in lower AHRR and high cyclic variability [26].

Despite the wealth of available literature or existing studies on the natural-gas dual-fuel engines, there is a considerable knowledge gap in the interplay between injector configuration, ambient condition and fuel-air premixing specific to H_2 dual-fuel combustion. Under the assumption that maximising the overlap between the fuel jets yields the best ignition performance, a converging setup using two single-hole injectors is used in this study. The effects of injection sequence, injection timing, and ambient gas temperature on the H2DDI ignition and combustion processes under DI CI engine relevant conditions are assessed. H_2 and *n*-heptane as a diesel surrogate were injected into a quiescent high-temperature, high-pressure charge within an optically accessible constant-volume combustion chamber (CVCC). Experimental diagnostics include high-speed schlieren imaging and pressure measurements.

Experimental details

Constant-volume combustion chamber

The experiments were conducted in an optically accessible CVCC with a quiescent high-pressure, high-temperature charge representative of CI engine conditions. The chamber is cubical with side dimensions of 114 mm, incorporating six interchangeable ports at the chamber faces. To avoid water condensation from the combustion products, the walls were kept at 403 K throughout the experiments. The H_2 and diesel injectors were installed in one side port, and a flat metal wall was installed in the opposite port. A mixing fan was installed in the top port to homogenize the ambient charge. Sapphire glass windows with 101.6 mm clear aperture were fitted in the remaining three ports (bottom port and ports perpendicular to the injector) to allow optical access. Fig. 1 (a) shows a schematic of the CVCC setup.

The pre-burn procedure for reaching high-pressure, high-temperature conditions in this CVCC has been detailed in Refs. [31–33,53]. In summary, a compressed lean mixture of C_2H_2, H_2, O_2 and N_2 was spark ignited to increase the in-chamber pressure and temperature, followed by a cool-down period as the heat is transferred to the surrounding chamber walls. The in-chamber pressure was monitored via a

Please cite this article as: Rorimpandey P et al., Hydrogen-diesel dual-fuel direct-injection (H2DDI) combustion under compression-ignition engine conditions, International Journal of Hydrogen Energy, https://doi.org/10.1016/j.ijhydene.2022.09.241

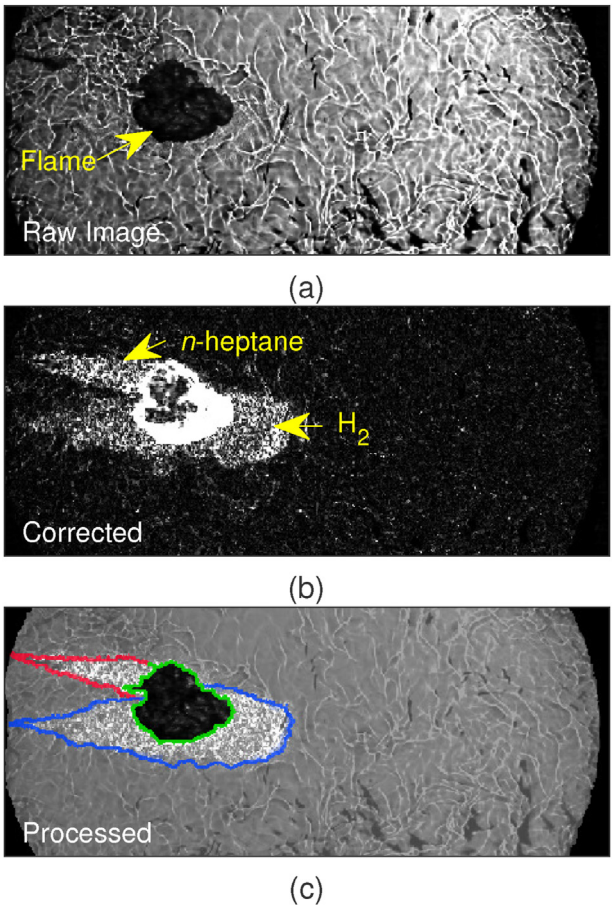

Fig. 4 – (a) Sample raw schlieren high-speed image, (b) image corrected by subtracting the pixel intensity values from the previous frame and (c) processed image showing the unreacted *n*-heptane (red) and H_2 (blue) jets, and reacted region (green). (For interpretation of the references to colour in this figure legend, the reader is referred to the Web version of this article.)

Table 3 – Summary of the investigated cases, their experimental settings and corresponding notations. Bold texts are the reference conditions.

Cases Investigated			
Case Name	Dwell Time		Ambient
	Pilot	Main	Temperature
H-0.07 ms-D/890K	**0.07 ms**	**-**	**890 K**
D-0.93 ms-H/890K	–	0.93 ms	890 K
D-1.93 ms-H/890K	–	1.93 ms	890 K
D-2.93 ms-H/890K	–	2.93 ms	890 K
H-1.07 ms-D/890K	1.07 ms	–	890 K
H-2.07 ms-D/890K	2.07 ms	–	890 K
H-3.07 ms-D/890K	3.07 ms	–	890 K
H-0.07 ms-D/820K	0.07 ms	–	820 K
H-0.07 ms-D/780K	0.07 ms	–	780 K

Experimental Parameters	
Parameter	Cases Investigated
Pilot-Main Injection Strategy	H-0.07 ms-D/890K
	D-0.93 ms-H/890K
	D-1.93 ms-H/890K
	D-2.93 ms-H/890K
Main-Pilot Injection Strategy	H-0.07 ms-D/890K
	H-1.07 ms-D/890K
	H-2.07 ms-D/890K
	H-3.07 ms-D/890K
Lower Ambient Gas Temperature	H-0.07 ms-D/890K
	H-0.07 ms-D/820K
	H-0.07 ms-D/780K

piezoelectric pressure transducer (Kistler 6052C with amplifier 5015A) to trigger the fuel injection event once the target in-chamber pressure (and hence temperature) condition was achieved during the cool-down phase. Fig. 2 shows the pressure history during a typical experiment run. For this study, the partial-pressure metered composition was tailored to achieve 21 vol% O_2 concentration after the pre-combustion, with an ambient density set to 23.8 kg/m^3.

The ambient temperature in the geometrical centre of the CVCC during the pre-combustion event was characterized using a thin-wire K-type thermocouple and is adopted as the representative charge temperature in this study. A baseline condition ambient temperature was set at 890 K, achieved by setting the target in-chamber pressure at SOI to 5.2 MPa. Lower ambient temperatures of 820 K and 780 K (4.6 MPa and 4.45 MPa, respectively) were used to investigate dual-fuel combustion under cooler temperature conditions (Section 2.5). Table 1 summarizes the experimental conditions. The H_2 ignition delay under tested conditions is considerably longer than that of *n*-heptane [34,35]. Therefore, it is reasonable to assume that the ignition of H_2 jet occurs due to its interaction with reacting or burnt *n*-heptane jet.

Injection settings

Two single-hole injectors with a converging configuration were used to separately inject the H_2 and diesel-pilot into the CVCC. Single-hole injectors were used instead of multi-hole injectors to simplify interpretation of experiments and avoid the complexities that arise from multiple jet interactions from the same injector. As shown in Fig. 1 (a), the H_2 injector was positioned at the centre of the port aligned with the port axis. The diesel injector orifice was positioned 12.3 mm above the H_2 injector orifice, at 12° relative to the H_2 injector axis. The jet axes intersect at 57.2 mm distance from the H_2 nozzle. Schlieren imaging suggests the jets start to interact as close as 28 mm from the H_2 injector or even closer when the diesel-pilot is injected before H_2 (see Section 3.2). Neat *n*-heptane was used as a single-component diesel-pilot fuel surrogate to reduce any compositional complexity and variables that can arise from using commercial fuels. Use of high cetane-number (low-octane) fuel is desired for the pilot-fuel to serve as a repeatable and reliable ignition source. The *n*-heptane fuel was injected at 70 MPa rail pressure using a commercial common rail injector (Bosch, solenoid, generation 2) equipped with a custom single-hole nozzle. The H_2 injector was derived from a modified commercial gasoline direct-injection (GDI, Bosch, HDEV5.1) injector that was fitted with a 0.58 mm single-hole diameter nozzle attachment [34]. The H_2 injector was supplied with compressed H_2 from a 1 dm^3 pressurized reservoir, which was charged using a pneumatic H_2

Please cite this article as: Rorimpandey P et al., Hydrogen-diesel dual-fuel direct-injection (H2DDI) combustion under compression-ignition engine conditions, International Journal of Hydrogen Energy, https://doi.org/10.1016/j.ijhydene.2022.09.241

compressor (Haskel with Zenobalti pressure controller). A reservoir pressure of 20 MPa was set, which resulted in roughly 14 MPa H_2 pressure upstream of the nozzle as a result of friction losses associated with the passage of gas through narrow channels within the injector [34].

The H_2 and *n*-heptane injectors were energized by independent external injector drivers (Zenobalti ZB-5012 and ZB-5014, respectively) with the timing set by a digital delay and pulse generator (Stanford Research Systems DG535). The hydraulic injection duration of H_2 and *n*-heptane were set to 3.3 ms and 0.7 ms, respectively, taking into account the delays associated with the opening and closing of the nozzles, and back pressure effects. The *n*-heptane mass flow was measured under nominally identical conditions using a Bosch-tube injection rate meter [36]. The injected amount of H_2 gas was determined by measuring the chamber pressure change when H_2 was injected [34]. Under the tested conditions, the injected fuel mass was 0.99 mg for *n*-heptane and 5.28 mg for H_2. Based on the fuels heating value, this means 6.4% of the energy share is from the *n*-heptane jet, with the rest from the H_2. Table 2 summarizes the experimental fuel injection conditions.

Optical diagnostics

Fig. 3 shows a schematic of the experimental optical arrangement. A Z-type schlieren imaging setup was used to detect the jet boundary and the high-temperature reaction zone. The roughly collimated light from a 150 W xenon arc lamp (Abet Technologies LS-150) was focused using a 50 mm plano-convex lens with a 75 mm focal length, which was then passed through a 2 mm aperture before collimation via a 108 mm f/6 parabolic mirror. The collimated light beam was directed through the CVCC, a second parabolic mirror, then into the high-speed camera through a series of mirrors. A 2 mm pin-hole aperture was placed between the second parabolic mirror and the camera lens at the beam focal point to enhance imaging sensitivity. The high-speed camera used is a Photron Fastcam SA5 equipped with an 85 mm f#1.8 AF-D Nikkor lens, operated at a 30,000 frames per second frame rate and a 1/525,000 s shutter speed, resulting in an image resolution of about 0.15 mm per pixel.

Schlieren imaging is an optical technique that is sensitive to refractive index gradients along the line-of-sight, induced by fuel evaporative cooling, mixing and combustion events, which are detectable as intensity variations on the image [32]. A high-temperature combustion event results in a steep refractive index gradient that can be identified as a darkened area on the schlieren image, as shown in Fig. 4 (a). The ambient gas (and hence the background schlieren pattern) was relatively stationary compared to the effects induced by the fast-moving jet. Therefore, the jet-induced schlieren effects can be discerned from the background structures by tracking the differences between video frames [39], as shown in Fig. 4 (b). The identified boundaries of the unreacted H_2 (blue) and *n*-heptane jets (red), along with the darkened burnt-zone region (green) are shown Fig. 4 (c).

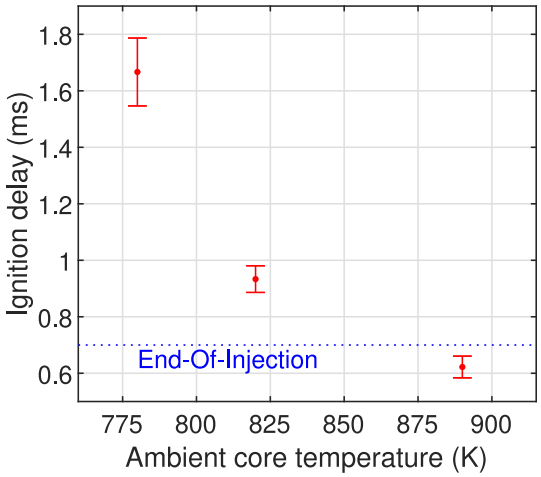

Fig. 5 – Schlieren-based ignition delay times of *n*-heptane at ambient temperatures of 780 K, 820 K and 890 K, with standard deviation shown as error bars.

Pressure trace and apparent heat release rate

In addition to the optical diagnostics, the pressure trace measurements acquired during the experiments were used to derive the AHRRs, to aid with the interpretation of results. For this study, we focus on the AHRR shape and features, which could be smeared by ensemble averaging in case of ignition delay variability. As a mitigation, before ensemble averaging, individual AHRR traces were shifted in time by the difference between the individual experiment realization ignition delay and the mean ignition delay. The following ensemble averaging formula was used:

$$\overline{\mathrm{AHRR}}(t) = \frac{1}{n}\sum_{i=1}^{n}\mathrm{AHRR}_i(t + t_{\mathrm{ID},i} - \overline{t_{\mathrm{ID}}}) \quad (1)$$

Table 4 – Average schlieren-based ignition delay time, the average times where 10% and 90% of the total heat release occurs (notated as CA10 and CA90, respectively), and the corresponding combustion duration of n-heptane at ambient temperatures of 890 K, 820 K and 780 K. Uncertainty provided as one standard deviation.

Ignition Delay and Combustion Duration of *n*-heptane				
Core temperature	Pilot ignition delay schlieren-based (ms)	CA10 (ms)	CA90 (ms)	Combustion duration CA10–CA90 (ms)
890 K	0.62 ± 0.04	0.79 ± 0.05	1.72 ± 0.40	0.93 ± 0.35
820 K	0.93 ± 0.05	0.91 ± 0.07	2.39 ± 0.41	1.48 ± 0.47
780 K	1.68 ± 0.12	1.10 ± 0.15	5.25 ± 1.37	4.15 ± 1.52

Please cite this article as: Rorimpandey P et al., Hydrogen-diesel dual-fuel direct-injection (H2DDI) combustion under compression-ignition engine conditions, International Journal of Hydrogen Energy, https://doi.org/10.1016/j.ijhydene.2022.09.241

Table 5 – Average pilot and main ignition delay times, relative to pilot-fuel and main-fuel SOI, for the reference case and pilot-main injection cases. Bold text indicates the reference case. The pilot ignition delay time relative to main-fuel SOI is omitted when the pilot-fuel autoignites prior to main-fuel SOI. Uncertainty provided as one standard deviation.

Ignition Delay Times				
Case name	Relative to pilot-fuel SOI		Relative to main-fuel SOI	
	Pilot (ms)	Main (ms)	Pilot (ms)	Main (ms)
H-0.07 ms-D/890K	**0.62±0.03**	**0.63±0.04**	**0.69±0.03**	**0.70±0.04**
D-0.93 ms-H/890K	0.58 ± 0.09	1.19 ± 0.09	–	0.26 ± 0.09
D-1.93 ms-H/890K	0.69 ± 0.03	2.30 ± 0.05	–	0.36 ± 0.05
D-2.93 ms-H/890K	0.66 ± 0.03	3.43 ± 0.14	–	0.49 ± 0.13

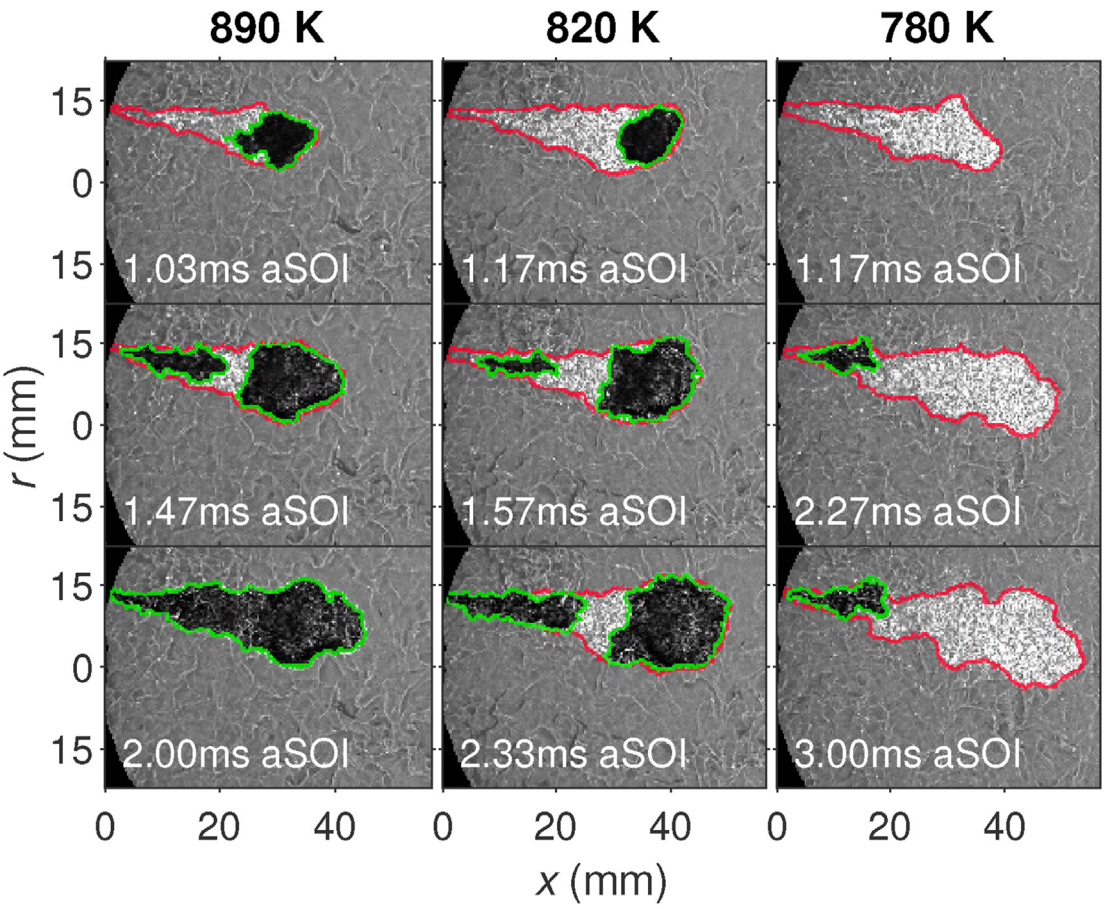

Fig. 6 – Processed schlieren images at select timings for *n*-heptane only injection, at ambient temperatures of 890 K (left), 820 K (middle), and 780 K (right). Overlaid are the unreacted *n*-heptane jet boundary (red) and the burn zone (green). Axial and radial distances from the H_2 injection nozzle are represented as *x* and *r*, respectively. (For interpretation of the references to colour in this figure legend, the reader is referred to the Web version of this article.)

where n denotes the total number of cycles, t_{ID} the ignition delay and the overline signifies ensemble-averaged quantities.

Experimental parameters and notations

The H2DDI combustion process was investigated under:

- *Pilot-main* injection strategy, where the pilot fuel (*n*-heptane) is injected prior to the main-fuel (H_2) start-of-injection (SOI).
- *Main-pilot* injection strategy, where the main fuel is injected before the pilot-fuel SOI.

This work uses the "pilot" and "main" fuel nomenclature widely used in dual-fuel combustion research, where "pilot-fuel" refers to the injection of diesel-like fuel serving as ignition source and "main-fuel" refers to the low ignition quality fuel that contributes the largest share of fuel LHV. This nomenclature is not to be confused with pilot and main injection in multiple-injection diesel engines.

Please cite this article as: Rorimpandey P et al., Hydrogen-diesel dual-fuel direct-injection (H2DDI) combustion under compression-ignition engine conditions, International Journal of Hydrogen Energy, https://doi.org/10.1016/j.ijhydene.2022.09.241

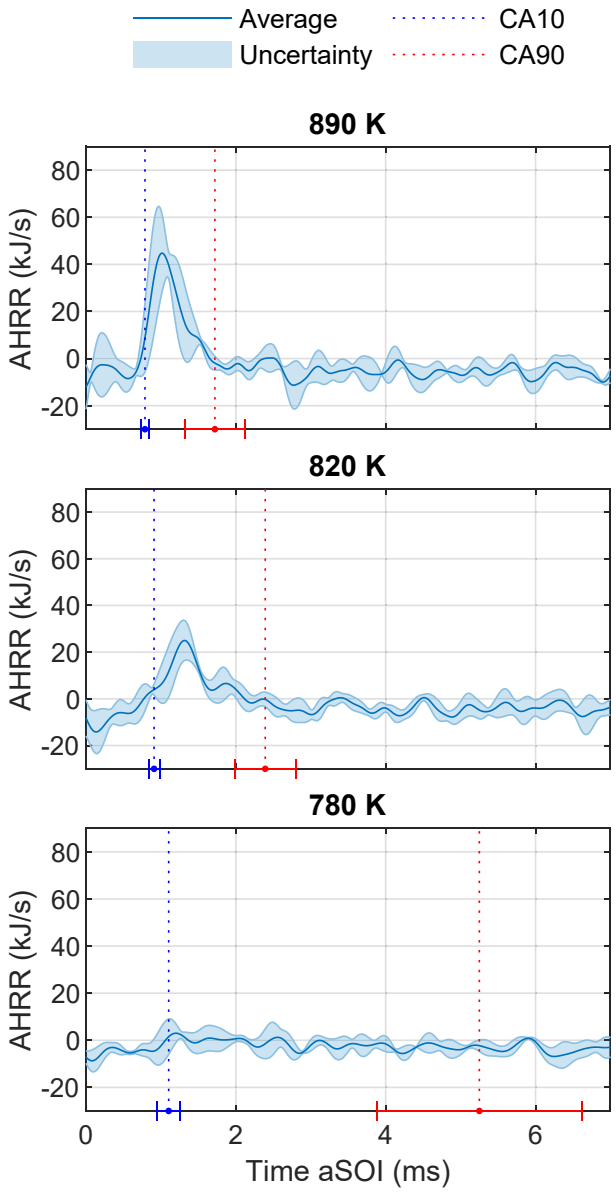

Fig. 7 – Averaged AHRR profiles for *n*-heptane only injection cases at ambient temperatures of 890 K (top), 820 K (middle) and 780 K (bottom). The average times where 10% and 90% of the total heat release occur (notated as CA10 and CA90, respectively) are plotted as blue and red dashed lines, respectively, with standard deviation shown along the time-axis. (For interpretation of the references to colour in this figure legend, the reader is referred to the Web version of this article.)

The dwell time, defined as the time between the primary and secondary actual SOI timings, was varied to investigate its effect. The fuel to which the dwell time refers depends on the parameter investigated. For a pilot-main case, the dwell time refers to the main-fuel SOI relative to the time after pilot-fuel SOI, and vice versa for a main-pilot case. As noted previously, the dwell time was set externally using a signal generator. Taking into account the electronic command delays and the actual opening and closing of the H_2 and diesel nozzles, dwell times of 0.93 ms, 1.93 ms and 2.93 ms were used for pilot-main cases, and dwell times of 1.07 ms, 2.07 ms and 3.07 ms were used for main-pilot cases. A near-simultaneous dual-injection case, where the pilot fuel was injected 0.07 ms after main-fuel SOI, was performed and used as a reference to compare results when investigating each parameter. In addition to the baseline ambient temperature of 890 K, the near-simultaneous dual-injection case was also tested under lower ambient temperatures of 820 K and 780 K. Furthermore, *n*-heptane only injection cases were also conducted in the three ambient temperatures as a reference. Each experimental case was repeated at least four times to eliminate outliers.

Table 3 summarizes the investigated cases, their settings and notations. For this study, the notation system adopted lays out the dwell time between the two fuels and the ambient temperature condition, with abbreviations of the diesel pilot (D) and H_2 main fuel (H) placed in the order of the injection sequence. For example, a main-pilot case with a dwell time of 1.07 ms and ambient temperature of 890 K is notated as 'H-1.07 ms-D/890K', while a pilot-main case with a dwell time of 0.93 ms at the same ambient temperature is notated as 'D-0.93 ms-H/890K'.

Ignition delay: pilot and main ignition

There may be two separate ignition events in dual-fuel combustion: the pilot-fuel autoignition and the main-fuel ignition that occurs after the jet interacts with the burnt pilot fuel. When separate ignition events occur, they are referred to as "pilot ignition" and "main ignition", respectively.

For this study, the pilot ignition is defined as the autoignition of *n*-heptane. While the autoignition of *n*-heptane leads to a distinct rise in the pressure trace at 890 K, the pressure rise becomes less defined at lower temperatures. This creates difficulty in identifying the pilot-ignition event from the pressure trace alone. Additionally, during the dual-fuel combustion, for the events where the pilot- and main-ignition events occur in close succession, only a single rise in the pressure trace can be detected. This prevents the discernment of the two ignition events and their ignition delay timings. For consistency reasons, high-speed schlieren images are used to determine the timing of the pilot ignition for all experimental cases. The pilot-ignition delay time is derived from the schlieren image frame where darkened high-temperature region first appears within the *n*-heptane jet.

For the dual-fuel cases, the schlieren effects from burnt pilot fuel obscures the main-fuel ignition, preventing an optical evaluation of the main ignition delay. Noting that a bulk of the heat release occurs during the main ignition, main-ignition time is derived based on the AHRR using thresholds, more precisely, the main ignition delay time was pinpointed as the latest time of AHRR not exceeding 18 kJ/s (above the noise floor of the AHRR data) before the 100 kJ/s was reached. This is motivated by the peak AHRR of pilot-only injections not exceeding 80 kJ/s. Note that by the above definition, in some instances, the main ignition is not strictly just the H_2 ignition,

Please cite this article as: Rorimpandey P et al., Hydrogen-diesel dual-fuel direct-injection (H2DDI) combustion under compression-ignition engine conditions, International Journal of Hydrogen Energy, https://doi.org/10.1016/j.ijhydene.2022.09.241

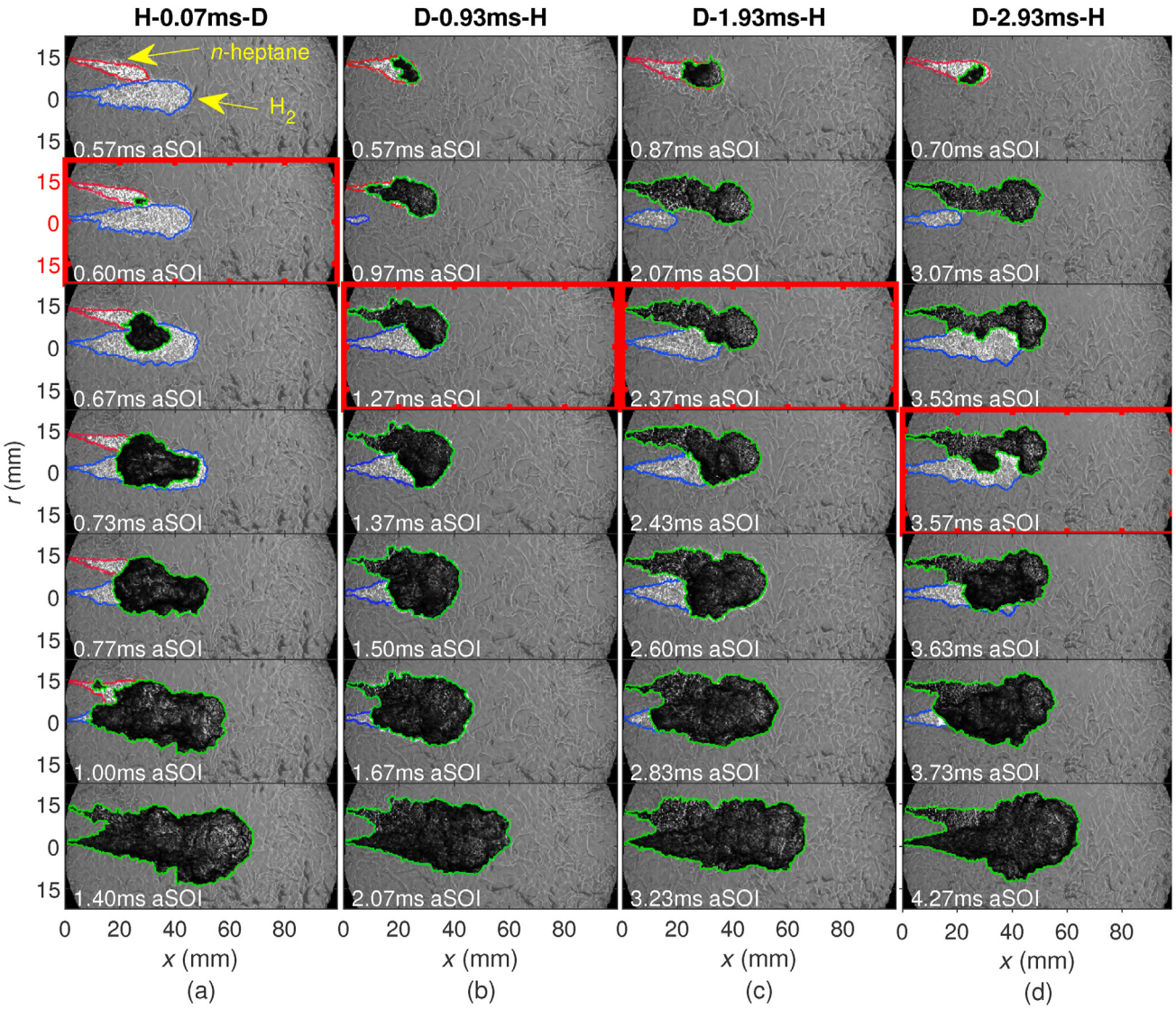

Fig. 8 – Processed schlieren images at select time instants for (a) reference case H-0.07 ms-D/890K, and pilot-main injection cases (b) D-0.93 ms-H/890K, (c) D-1.93 ms-H/890K and (d) D-2.93 ms-H/890K. Highlighted are the *n*-heptane jet boundary (red), H_2 jet boundary (blue), and high-temperature flame (green). Axial and radial distances from the injection nozzle are represented as *x* and *r*, respectively. The first frame following pressure-based ignition delay time is outlined by a red border. Time sequence is relative to the earlier injection (*i.e.*, *n*-heptane SOI). (For interpretation of the references to colour in this figure legend, the reader is referred to the Web version of this article.)

as the heat release from *n*-heptane autoignition also contributes if the two ignition events occur in quick succession.

Results and discussion

Combustion characteristic of n-heptane

The *n*-heptane combustion (in the absence of H_2) was characterized at different ambient temperatures in terms of ignition delay, burnt-zone evolution and AHRR. Fig. 5 and Table 4 present the average and standard deviation of schlieren-based ignition delay of *n*-heptane at various ambient temperatures relative to different SOI timings. The ignition delay of *n*-heptane increases with lower temperature [40], increasing by a factor of 2.8 as the temperature decreases.

Fig. 5 shows ignition occurs before the EOI at the highest temperature (*i.e.* negative ignition dwell [41]). This is noteworthy since aEOI, the entrainment wave rapidly leans out the jet, which was shown to impact the jet ignition relative to a longer injection [42] and change the burnt gas temperature that the interacting H_2 jet will experience.

Fig. 6 provides sample schlieren images for *n*-heptane-only case, highlighting the unreacted jet (red) and the flame (green) development at different temperatures. The main difference is in the ignition location and the spreading rate of combustion from the initial ignition spot - both of these effects can impact the main-fuel ignition. At 890 K, the autoignition

Please cite this article as: Rorimpandey P et al., Hydrogen-diesel dual-fuel direct-injection (H2DDI) combustion under compression-ignition engine conditions, International Journal of Hydrogen Energy, https://doi.org/10.1016/j.ijhydene.2022.09.241

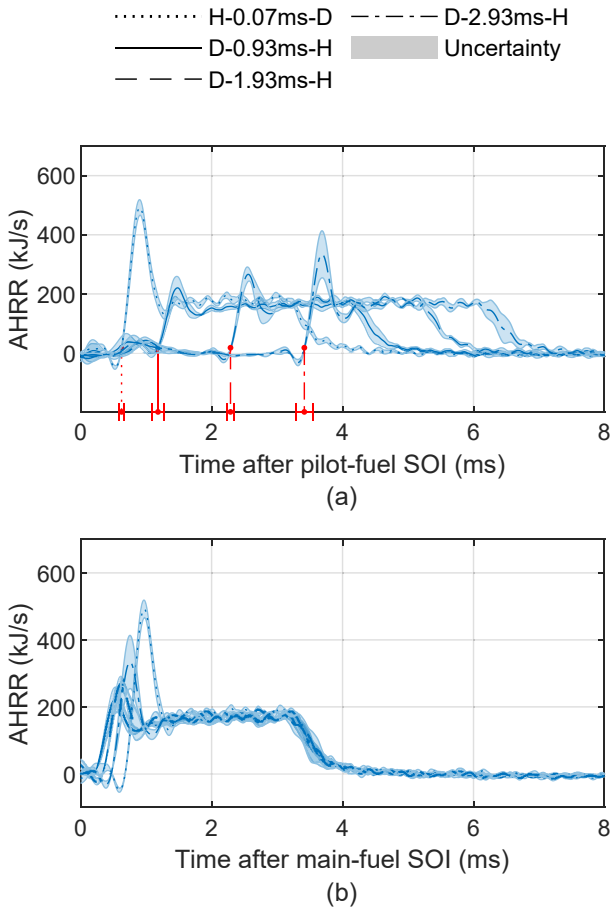

Fig. 9 – Averaged AHRR relative to (a) pilot-fuel SOI and (b) main-fuel SOI for reference case H-0.07 ms-D/890K, and pilot-main injection cases D-0.93 ms-H/890K, D-1.93 ms-H/890K and D-2.93 ms-H/890K, with the AHRR variability between experimental runs shown. Ignition delay uncertainty of each case shown by red line along time-axis of (a). See text for further details. (For interpretation of the references to colour in this figure legend, the reader is referred to the Web version of this article.)

occurred at the jet head prior to the separate ignition spot aEOI in the near-nozzle jet tail. The two ignited regions merged over time. A similar ignition process was observed at 820 K, but the two ignited regions did not combine within the observation period. At 780 K, the ignition only occurred aEOI near the nozzle and failed to spread. The mixture in the jet head has the longest residence time in the hot environment and initially a favourable fuel-to-air ratio [43], however, it rapidly leans out after EOI. This is why this region is the first to autoignite at 890 K, but becomes too lean to autoignite at 780 K. Regions near the injector may remain fuel-richer longer due to the EOI ramp-down and the injector needle-bouncing injecting low-velocity droplets. These can lead to separate ignition pockets [44] visible near-nozzle at 890 K and 820 K and the sole source of ignition at 780 K.

The pilot-only ignition timing and combustion phases are evaluated based on AHRR (Fig. 7) [12,34,45]. The peak AHRR decreases by a factor of 2 from 890 K to 820 K, while no AHRR peak is distinguishable from the AHRR profile at 780 K. These trends are contrary to the traditional long-injection diesel combustion with increasing premixed peak at a longer ignition delay; this indicates that the studied pilot-injections become significantly lean before ignition, which reduces the overall fuel reactivity and slows the combustion.

The cyclic variability of the pressure-derived AHRR (shaded region, ±1 standard deviation) is low at higher temperatures, while the AHRR cannot be distinguished from noise at 780 K. Fig. 7 shows the timings where 10% (CA10) and 90% (CA90) of the cumulative heat release occur, analogous to typical engine study notations, serving as reference for the parametric variation results presented next. Table 4 provides the ignition delay and combustion duration (defined as the time between CA10 and CA90), showing that the time of CA10, CA90 and combustion duration increase with decreasing ambient temperature, with increased cyclic variability.

Pilot-main injection strategy

Injecting the pilot fuel before the main-fuel SOI allows the pilot jet to develop before interacting with the main jet. In all tested pilot-main injection cases with a dwell time of 0.93 ms after *n*-heptane SOI (D-0.93 ms-H/890K) and longer, the *n*-heptane jet has ignited before H_2 SOI. Fig. 8 shows selected high-speed schlieren images for the reference case H-0.07 ms-D/890K and the pilot-main injection cases D-0.93 ms-H/890K, D-1.93 ms-H/890K and D-2.93 ms-H/890K, exemplifying the key instances of flame evolution referenced to the pilot-fuel SOI (*i.e.*, *n*-heptane SOI).

For the reference case H-0.07 ms-D/890K (Fig. 8 (a)), at 0.60 ms aSOI, the *n*-heptane jet ignites outside the H_2 jet boundary. The ignition kernel originates from the head section and one image frame later, the H_2 jet ignited at around 28 mm from the H_2 nozzle. Despite the line-of-sight diagnostic limitations, the evolution of the burnt zone after ignition, in addition to the steep pressure rise at this timing, gives confidence that the H_2 jet is indeed burning. Also for the pilot-main cases, the H_2 jet ignites after interacting with the burnt *n*-heptane jet.

Fig. 9 provides the averaged AHRR profiles for the reference and pilot-main injection strategy. Table 5 states the average pilot and main ignition delay times derived based on high-speed schlieren imaging and pressure data, respectively. For the reference case H-0.07 ms-D/890K (Fig. 9 (a)), the unchanged ignition delay relative to pilot-only case (Section 3.1) indicates that the H_2 jet does not impact the ignition of *n*-heptane. The *n*-heptane and H_2 ignite nearly simultaneously leading to a single AHRR peak with magnitude of roughly 2.5 times the steady-state AHRR of 190 kJ/s. During the steady-stage mixing-controlled phase, the AHRR matches the heating value of H_2 inflow at measured injection rate of 1.56 mg/ms [34]. For the pilot-main cases, two distinct AHRR peaks are visible, which correspond to the pilot- and main-ignition events. The pilot ignites before interacting with H_2 jet, with an unchanged ignition delay relative to pilot-only case, within experimental uncertainty. Subtle differences in the peak AHRR and the ignition timing after the interaction with pilot-jet are best visible when the AHRR profiles are plotted relative to main-fuel SOI (Fig. 9 (b)). The main-ignition delay and the

Please cite this article as: Rorimpandey P et al., Hydrogen-diesel dual-fuel direct-injection (H2DDI) combustion under compression-ignition engine conditions, International Journal of Hydrogen Energy, https://doi.org/10.1016/j.ijhydene.2022.09.241

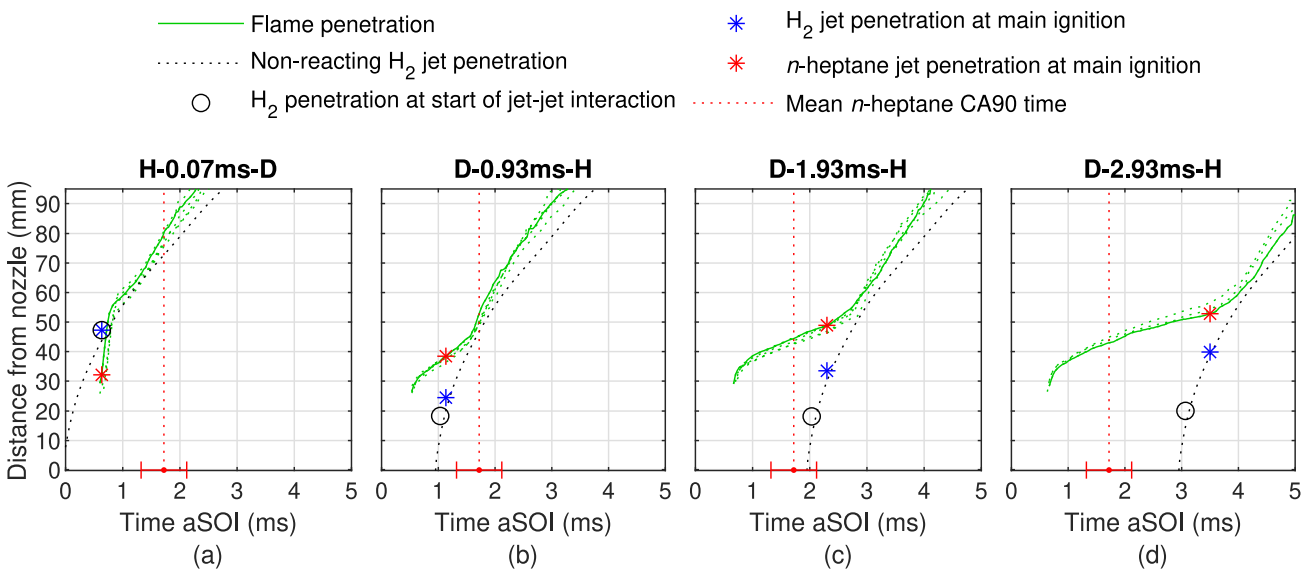

Fig. 10 – Flame penetration for (a) reference case H-0.07 ms-D/890K, and pilot-main injection cases (b) D-0.93 ms-H/890K, (c) D-1.93 ms-H/890K and (d) D-2.93 ms-H/890K. See text for detailed explanation of the plot.

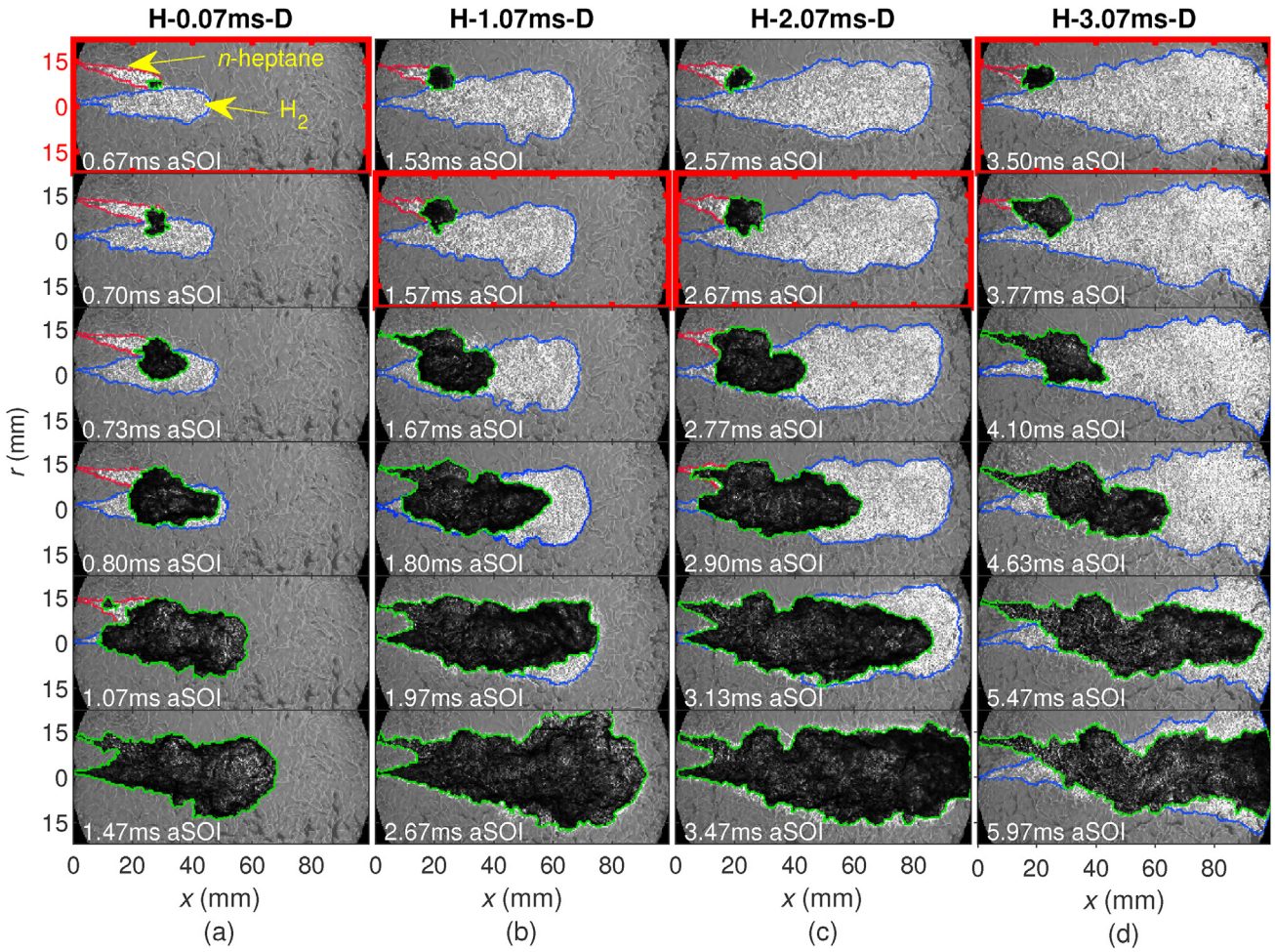

Fig. 11 – Processed schlieren images at select time instants for (a) reference case H-0.07 ms-D/890K, and main-pilot injection cases (b) H-1.07 ms-D/890K, (c) H-2.07 ms-D/890K and (d) H-3.07 ms-D/890K. Highlighted are jet boundaries for *n*-heptane (red), H_2 (blue), and high-temperature flame (green). Axial and radial distances from the injection nozzle are represented as *x* and *r*, respectively. The first frame following pressure-based ignition delay time is outlined by a red border. Time sequence is relative to the earlier injection (*i.e.*, H_2 SOI.). (For interpretation of the references to colour in this figure legend, the reader is referred to the Web version of this article.)

Please cite this article as: Rorimpandey P et al., Hydrogen-diesel dual-fuel direct-injection (H2DDI) combustion under compression-ignition engine conditions, International Journal of Hydrogen Energy, https://doi.org/10.1016/j.ijhydene.2022.09.241

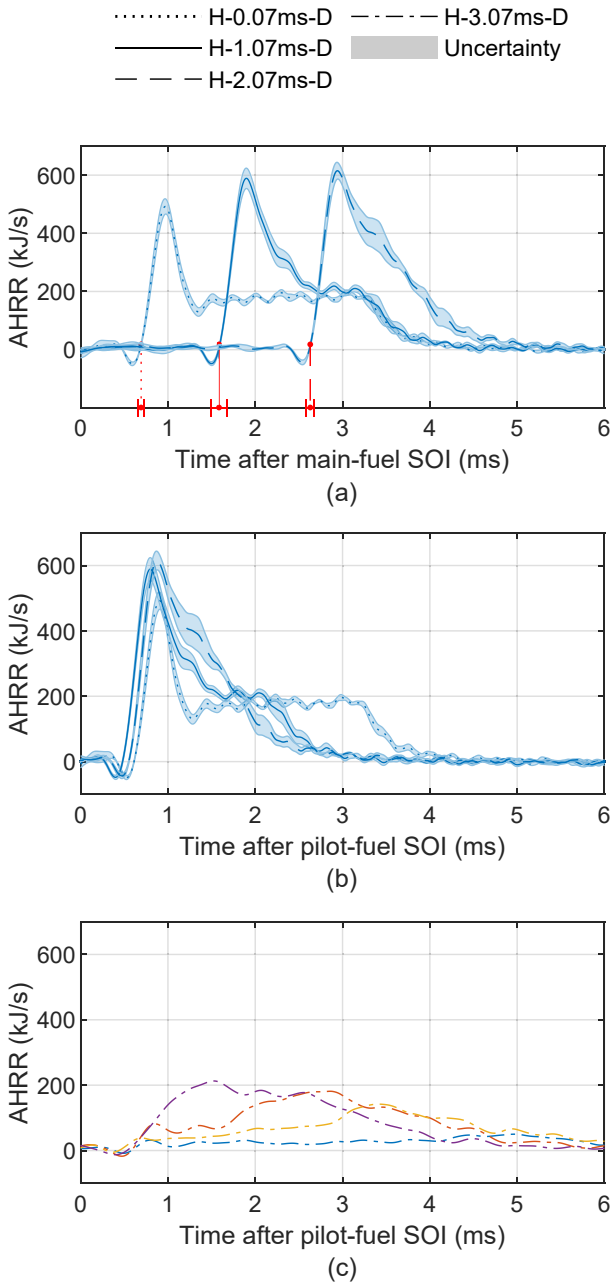

Fig. 12 – Averaged AHRR relative to (a) main-fuel SOI and (b) pilot-fuel SOI for reference case H-0.07 ms-D/890K and main-pilot injection cases H-1.07 ms-D/890K and H-2.07 ms-D/890K. AHRR for H-3.07 ms-D/890K case individual runs (c). All times relative to pilot-fuel SOI. Ignition delay uncertainty of each case shown by red line along time-axis of (a). See text for more details. (For interpretation of the references to colour in this figure legend, the reader is referred to the Web version of this article.)

peak AHRR increase with a longer dwell time, as further discussed below.

To aid further interpretation, Fig. 10 provides the schlieren-derived flame penetration trends (represented by a solid green line) plotted relative to the pilot-fuel SOI. The experimental run with the pilot-ignition delay closest to the average is presented with solid lines while other runs are showed with dashed lines and show repeatable trends. A non-reacting H_2-only-case jet penetration (represented using a dashed black line) is provided as a reference. Note that in dual-fuel cases, the pilot-fuel slip-stream effect and the jet expansion due to combustion might lead to a faster H_2-jet penetration than the non-reactive reference [46]. The H_2 and *n*-heptane jet penetrations during their main-ignition timings are marked in blue and red, respectively. The H_2 jet penetration when it first appears to interact with the *n*-heptane jet is marked by a circle. The time of pilot-only case CA90 (*c.f.* Section 3.1) is indicated using a vertical red dashed line.

For the reference case H-0.07 ms-D/890K (Fig. 10 (a)), the H_2 jet ignites upstream of its jet tip at about 0.6 ms aSOI. The flame penetration reached the H_2 jet tip by 1.0 ms aSOI, after which the penetration is marginally faster than the non-reacting jet reference. For the pilot-main cases, the H_2 jet starts to interact with burnt pilot-fuel at the tip, where it also ignites shortly after. Sometime after the ignition of the main jet, the inflection point in the flame penetration indicates the burnt H_2 jet has accelerated beyond the pilot-jet. The similarity in flame penetration trends with different dwell times indicates that the H_2 jet momentum drives the penetration of the burnt zone later after ignition. Fig. 10 also shows an increasing time separation and distance between the initial jet-jet interaction (black circle) and ignition (star symbols) with increasing dwell time. These findings indicate that at a longer dwell time, a longer jet-jet interaction is required to ignite the H_2 jet because of the cooler *n*-heptane jet at the time of interaction.[2] The prolonged jet-jet interaction period before H_2 jet ignition increases the amount of the injected and mixed H_2 as it ignites, which explains the higher AHRR at ignition (Fig. 9). The reference case is an exception to this trend because the time of jet-jet interaction is governed by the slower pilot-fuel jet penetration, not the H_2 jet penetration.

Main-pilot injection strategy

This section investigates the effects of dwell time on flame evolution and AHRR in a main-pilot strategy. Fig. 11 provides the sample high-speed images for the cases H-0.07 ms-D/890K, H-1.07 ms-D/890K, H-2.07 ms-D/890K and H-3.07 ms-D/890K, using the same colour scheme, format, and annotation used in Section 3.2. In all main-pilot cases, the *n*-heptane jet autoignites before interacting with the H_2 jet at approximately 28 mm from the H_2 nozzle. The amount of H_2-air mixture injected before jet-jet interaction increases with a longer dwell time. The combustion propagates from the point of contact between the jets towards the nozzle and jet tip as it engulfs the unburnt H_2 jet regions. At the longest tested dwell (H-3.07 ms-D/890K), the H_2 flame fails to propagate towards the H_2 jet tip and radial periphery regions. The reasons for the limited extent of flame propagation at longest dwell will be discussed in Section 3.3.1.

The impacts of dwell time and flame evolution on AHHR are shown in Fig. 12, relative to pilot- and main-fuel SOI. At the

[2] The ambient gas temperature decreases roughly 0.15 K/ms - this effect on the jet-jet interaction is considered negligible.

Table 6 – Average pilot and main ignition delay times, relative to pilot-fuel and main-fuel SOI, for the reference case and main-pilot injection cases. Bold texts indicate reference case. Uncertainty provided as one standard deviation.

Ignition Delay Times				
Case name	Relative to pilot-fuel SOI		Relative to main-fuel SOI	
	Pilot (ms)	Main (ms)	Pilot (ms)	Main (ms)
H-0.07 ms-D/890K	**0.62±0.03**	**0.63±0.04**	**0.69±0.03**	**0.70±0.04**
H-1.07 ms-D/890K	0.46 ± 0.10	0.51 ± 0.10	1.55 ± 0.09	1.59 ± 0.09
H-2.07 ms-D/890K	0.50 ± 0.02	0.56 ± 0.04	2.57 ± 0.03	2.64 ± 0.04
H-3.07 ms-D/890K	0.42 ± 0.05	0.50 ± 0.04	3.49 ± 0.06	3.57 ± 0.04

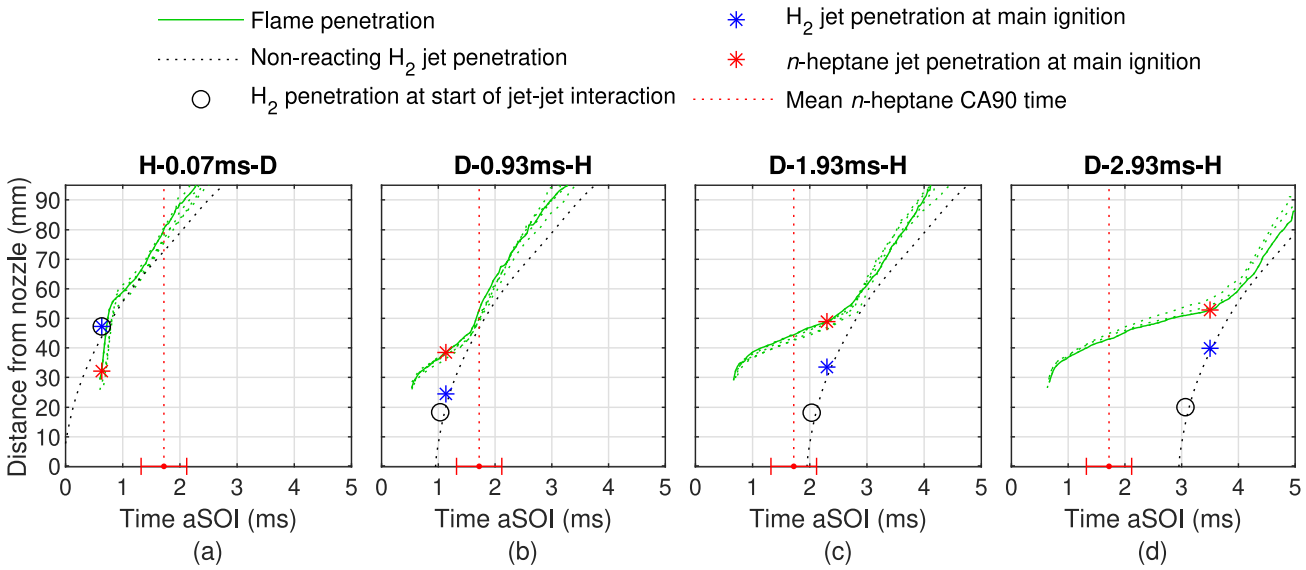

Fig. 13 – Flame penetration for (a) reference case H-0.07 ms-D/890K and main-pilot injection cases (b) H-1.07 ms-D/890K, (c) H-2.07 ms-D/890K (all runs shown by green solid or dashed lines) and (d) H-3.07 ms-D/890K (all runs shown by solid lines, with the line colors selected to match that of their AHRR profiles in Fig. 12 (c)). Non-reacting H_2 jet penetration shown as black dashed lines. Markers used to identify jet penetration of H_2 (blue) and *n*-heptane (red) at H_2 ignition. Circle marker used to identify H_2 jet penetration at start of interaction with *n*-heptane jet. Time sequence starts relative to first SOI (*i.e.*, H_2 SOI). Mean CA90 time of *n*-heptane shown by red dash line, with standard deviation shown along the time-axis. (For interpretation of the references to colour in this figure legend, the reader is referred to the Web version of this article.)

Table 7 – Input parameters used to set up the Musculus and Kattke jet model [42,50] simulating H_2 mixing aEOI.

Jet Model Input Parameters	
Ambient gas temperature	890 K
Ambient gas density	23.8 kg/m^3
Fluid (H_2) density	3.13 kg/m^3
Nozzle diameter	0.58 mm
Injection velocity	2991 ms^{-1}
Ramp down time EOI	0.05 ms
Jet angle	25°

longest dwell (H-3.07 ms-D/890K), the AHRR is not ensemble averaged due to the large cyclic variability —single-cycle traces are shown instead. All cases show a single AHRR peak due to the close succession of pilot- and main-ignition events. The main-jet residence time before ignition increases with a longer dwell time (delayed interaction with pilot), which increases the AHRR analogous to conventional diesel combustion at longer ignition delay. However, at longer dwells, the mixing-controlled combustion phase (steady AHRR phase) becomes less defined since ignition is too close to the EOI. The larger mass of H_2 available at ignition also prolongs the premixed-burn phase.

It is noteworthy that the pilot- and main-ignition delays summarized in Table 6 show a shorter pilot-ignition delay for the main-pilot cases than in the pilot-only case at the same ambient temperature (Section 3.1). As noted in previous studies [46–48], the increased velocity and turbulence that the first injection produces can enhance the mixing of the subsequent injection. In present case, the turbulence from the H_2 jet may increase the fuel-air mixing rate of the approaching *n*-heptane jet. An alternative explanation is that the H_2 jet homogenizes the temperature difference between the cooler gases near the vessel walls and hotter gasses in the core; this changes the conditions that the pilot jet experiences in the initial penetration stages. The exact mechanism requires further investigation to confirm.

Fig. 13 provides the schlieren-derived flame penetration trends plotted relative to the main-fuel SOI, following the

Please cite this article as: Rorimpandey P et al., Hydrogen-diesel dual-fuel direct-injection (H2DDI) combustion under compression-ignition engine conditions, International Journal of Hydrogen Energy, https://doi.org/10.1016/j.ijhydene.2022.09.241

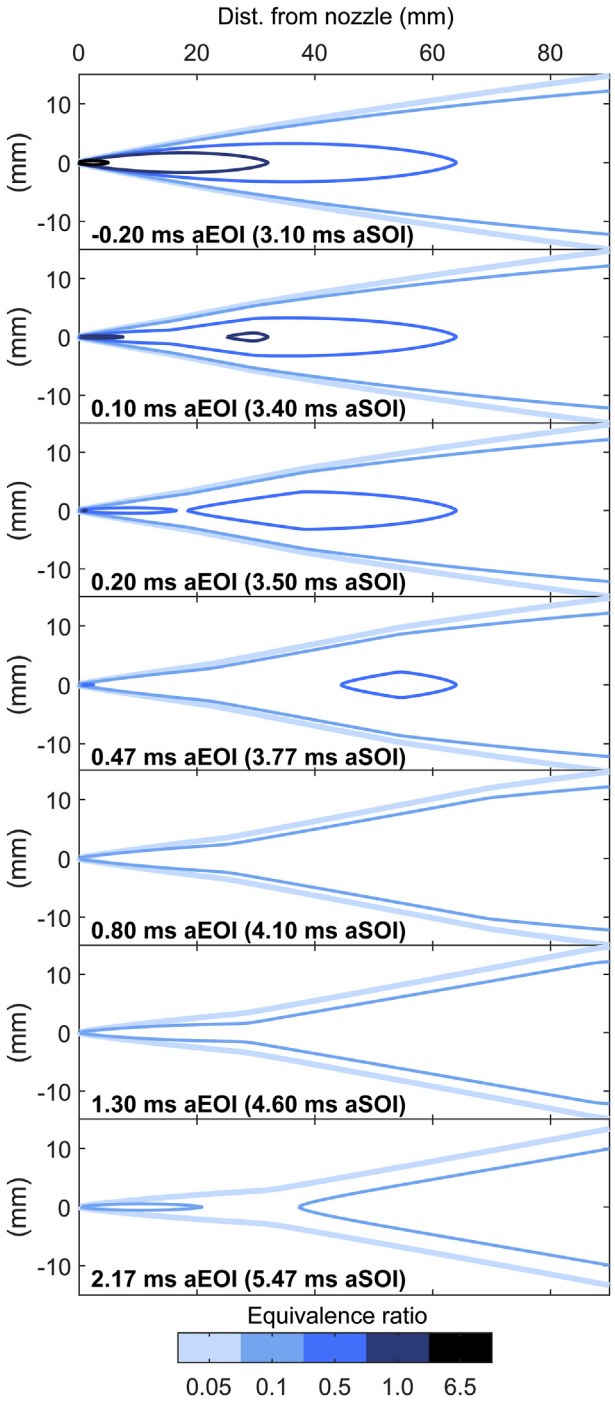

Fig. 14 – Time sequence of the modelled fuel spray aEOI, based on the Musculus and Kattke control-volume jet model [42,50], showing the change in equivalence ratio across the jet body.

same convention as Fig. 10. A non-reacting H_2-only-case jet penetration is also provided as reference. The results show that the H_2 jet penetration at the time of ignition increases with a longer dwell time, which is expected because of the increased delay when H_2 starts interacting with the burnt pilot fuel. The flame penetration of the main-pilot cases occurs in a repeatable manner after ignition. The case with the longest tested dwell (H-3.07 ms-D/890K) is an exception to this trend as it shows large cyclic variability in its flame penetration path. Referring back to the AHRR profiles for the case H-3.07 ms-D/890K (Fig. 12 (c)), it is notable that the magnitude of the peak AHRR roughly corresponds to the rate at which the flame proceeded throughout the jet volume. A noteworthy observation is that, unlike other main-pilot cases, the pilot fuel ignites after the main-fuel EOI for case H-3.07 ms-D/890K. This suggests that the fuel-air mixing effects of aEOI contribute to inconsistent flame penetration paths and AHRR profiles for the longest dwell.

Pilot-fuel injection after main-fuel EOI

This section investigates the EOI effects on the fuel-air mixing in the case of the longest dwell, considering previous studies have reported the rapid leaning out of the fuel jet by the entrainment aEOI [42,44,49]. A jet model based on the Musculus and Kattke control-volume jet model [42,50] is used to assess the EOI effects on the H_2-air mixture at the time of interaction with *n*-heptane jet. All model parameters were kept the same as in the experiments (summarized in Table 7), and the jet cone angle was tuned to match the modelled and the experimental penetration trends. A spray cone angle of 25° was found to yield a good agreement for the jet penetration between the model and experimental data. The approach of tuning model cone angle to match the experimental penetration was previously validated to be capable of generating accurate mixture predictions of vaporized sprays [51]. The good agreement between the very lean modelled contour with the experimental jet boundary (not shown) provides further confidence in the model results.

Fig. 14 shows the modelled equivalence ratio (φ) distributions at selected timesteps to provide indications of the mixture states of the experimental frames in Fig. 11 (d). The φ contours are calculated based on 21% ambient O_2 concentration. The plotted contour levels are motivated by the H_2 flammability limits of $\varphi = 0.1$ and 6.5 at standard temperature and pressure [6] as rough estimates of the flammable mixture extent in the jet, neglecting the pressure/temperature effects [52]. Fig. 14 shows that the near-nozzle fuel concentration continuously decreases aEOI, which suggests the jet-jet interaction occurs in very lean H_2 jet regions that are less favourable for flame propagation. This explains the experimentally observed slower combustion spreading, cyclic variability and the unburnt zones remaining late after ignition. It is emphasized that whilst the simplified model provides useful insights, the model does not provide an exact simulation of the fuel-air mixture distribution within the H_2 jet as several jet model parameters required estimation. The model also does not reproduce cyclic variations and other relevant processes, including turbulence-chemistry interaction, which can affect the ignition of the fuel mixtures.

Cases with lower ambient gas temperature

This section investigates the ambient temperature effects on the flame evolution and AHRR of the dual-fuel cases. Fig. 15 shows selected high-speed schlieren images for the reference case H-0.07 ms-D/890K and the lower ambient temperature cases H-0.07 ms-D/820K and H-0.07 ms-D/780K, following the same convention as Fig. 8. When comparing the

Please cite this article as: Rorimpandey P et al., Hydrogen-diesel dual-fuel direct-injection (H2DDI) combustion under compression-ignition engine conditions, International Journal of Hydrogen Energy, https://doi.org/10.1016/j.ijhydene.2022.09.241

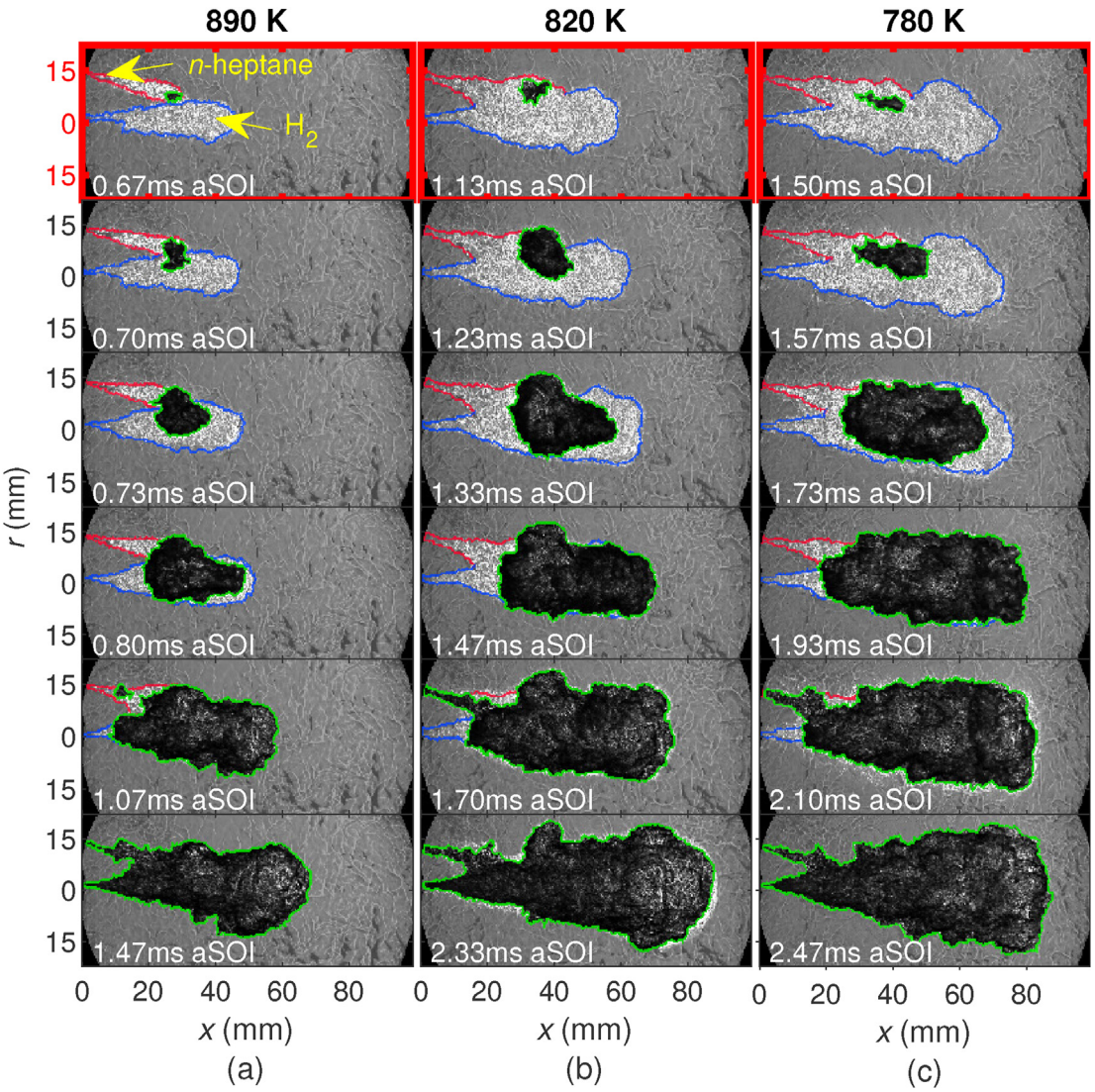

Fig. 15 – Processed schlieren images at select time instants for (a) reference case H-0.07 ms-D/890K, and lower ambient temperature cases (b) H-0.07 ms-D/820K and (c) H-0.07 ms-D/780K. Highlighted are the *n*-heptane jet boundary (red), H_2 jet boundary (blue), and high-temperature flame (green). Axial and radial distances from the injection nozzle are represented as *x* and *r*, respectively. The first frame following pressure-based ignition delay time is outlined by a red border. Time sequence starts relative to H_2 SOI. (For interpretation of the references to colour in this figure legend, the reader is referred to the Web version of this article.)

schlieren images of the three cases, the initial ignition spot locates externally to the H_2 jet boundary at 890 K but appears to emerge at a location that is closer to, or within the H_2 jet boundary at lower temperatures. Recognising the line-of-sight limitation of schlieren diagnostics that prevents the determination of the exact kernel locations in a three-dimensional space, the shift in the relative positioning of the ignition spot, nevertheless, suggests that at lower ambient temperature the *n*-heptane jet autoignites after interacting with the H_2 jet. The flame penetration plots presented for previous variations are not informative for the ambient temperature cases and are not presented.

Fig. 16 presents the averaged AHRR traces for the ambient temperature variation cases, with Table 8 summarizing the pilot and main ignition delay times. The statistically indifferent ignition delay of the tested ambient temperature variation cases relative to the pilot-only cases (Section 3.1) indicates that the interaction between the H_2 and *n*-heptane jets does not affect the pilot ignition. Similarly to previous variations that led to increased main-fuel ignition delay, the increase in ignition delay and, therefore, the corresponding residence time of the main jet before ignition also increase the AHRR at lower temperatures. The mixing-controlled combustion phase becomes less defined at the lowest temperature (H-0.07 ms-D/780K). This may be partly attributable to the ensemble averaging method (*e.g.*, shifting the AHRR to align with the ignition time shifts relative to the EOI, which might introduce non-physical variability in late combustion stages). The less-defined mixing-controlled AHRR can also be attributed to the variability in the *n*-heptane ignition location at 780 K (Fig. 17)—the ignition location impacts the premixed burn transient that can last until nearly the EOI.

Please cite this article as: Rorimpandey P et al., Hydrogen-diesel dual-fuel direct-injection (H2DDI) combustion under compression-ignition engine conditions, International Journal of Hydrogen Energy, https://doi.org/10.1016/j.ijhydene.2022.09.241

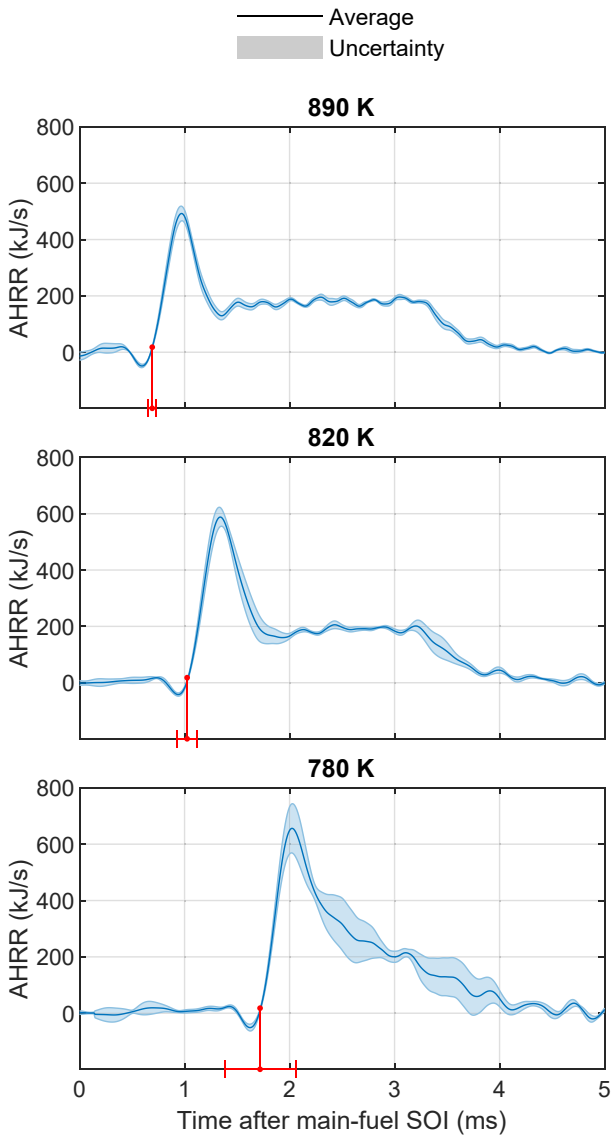

Fig. 16 – Averaged AHRR relative to main-fuel SOI at varying ambient gas temperatures: H-0.07 ms-D/890K (top), H-0.07 ms-D/820K (middle) and H-0.07 ms-D/780K (bottom). Ignition delay uncertainty of each case shown by red line along time-axis. (For interpretation of the references to colour in this figure legend, the reader is referred to the Web version of this article.)

Fig. 17 (a) shows select schlieren frames from three experimental runs of case H-0.07 ms-D/780K to highlight the source of cyclic variations. The *n*-heptane ignition may originate from the jet head, jet tail, as well as both jet-head and jet-tail sections. The corresponding AHRR profiles, which are provided in Fig. 17 (b), show that the AHRR profile changes depending on the initial ignition kernel location and the ignition delay of each run. The AHRR profile of the run in Fig. 17 (a)(i), which exhibits jet-head ignition and shorter-than-average ignition delay, has a distinct premixed combustion AHRR peak followed by a steady diffusion flame period that is similar to the higher temperature cases. When ignition occurs later, in the near-nozzle region (Fig. 17 (a)(ii)) or with two ignition kernels (Fig. 17 (a)(iii)), the peak AHRR profile is wider and slowly decays to the steady AHRR value that it reaches around the EOI. The wider AHRR peak profile with a reduced amplitude can be associated with a slower flame evolution through the H_2 jet volume. The reasons for slower evolution are two-fold: (1) flame propagating through an overall leaner H_2 mixture due to the delayed ignition; (2) the ignition initially occurs in a mixture less favourable for flame propagation leading to slower combustion spreading. The relative importance of these mechanisms needs further examination.

Summary and conclusions

The ignition and combustion characteristics of intersecting H_2 and diesel jets were investigated under engine-relevant high-pressure high-temperature conditions in an optically accessible constant-volume combustion chamber (CVCC) using high-speed schlieren imaging and pressure trace analysis. The H_2 (main fuel) and *n*-heptane (pilot fuel, diesel surrogate) were injected using single nozzle injectors arranged with a converging angle of 12°. The pilot fuel accounted for 6% of the injected fuel energy. The effects of ambient temperature and injection sequence (pilot-main injection, main-pilot injection, and near-simultaneous injections) on the ignition and combustion properties were investigated and compared to reference cases with only *n*-heptane injections under otherwise unchanged conditions.

The following conclusions apply under the conditions investigated in this work:

Table 8 – Average pilot and main ignition delay times relative to pilot-fuel and main-fuel SOI, respectively, for the reference case and lower temperature cases. Ignition delay of *n*-heptane (discussed in Section 3.1) is also shown for reference. Bold texts indicate reference case. Uncertainty provided as one standard deviation.

Ignition Delay Times			
Case name	Pilot ignition relative to pilot-fuel SOI (ms)	Main ignition relative to main-fuel SOI (ms)	*n*-heptane only ignition delay (ms)
H-0.07 ms-D/890K	**0.62±0.03**	**0.70±0.04**	**0.62±0.04**
H-0.07 ms-D/820K	0.93 ± 0.07	1.03 ± 0.09	0.93 ± 0.05
H-0.07 ms-D/780K	1.42 ± 0.19	1.73 ± 0.34	1.68 ± 0.12

Please cite this article as: Rorimpandey P et al., Hydrogen-diesel dual-fuel direct-injection (H2DDI) combustion under compression-ignition engine conditions, International Journal of Hydrogen Energy, https://doi.org/10.1016/j.ijhydene.2022.09.241

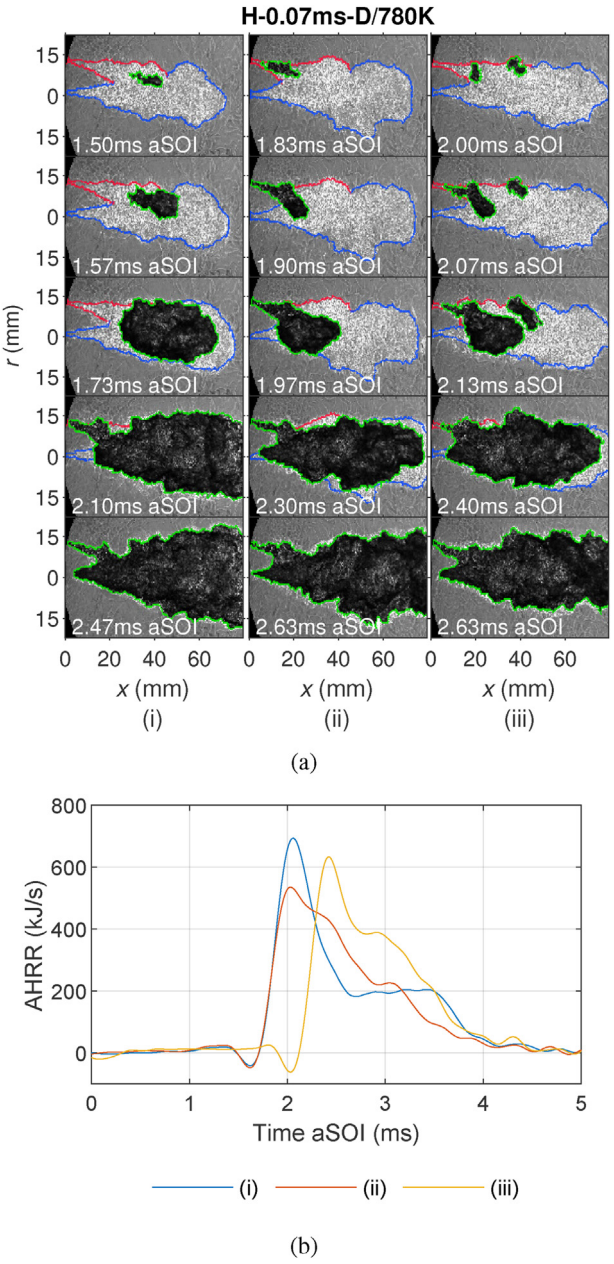

Fig. 17 – (a) High-speed images from three runs for H-0.07 ms-D/780K, showing ignition originating from the *n*-heptane jet head-section (i), tail-section (ii), as well as both head and tail-section (iii). Highlighted are the *n*-heptane jet boundary (red), H_2 jet boundary (blue) and high-temperature flame (green). (b) The corresponding AHRR of the H-0.07 ms-D/780K experimental runs shown in (a). (For interpretation of the references to colour in this figure legend, the reader is referred to the Web version of this article.)

1. The pilot-fuel ignition is not influenced by the interaction with H_2 jet. The quenching of pilot-fuel when interacting with natural-gas jets, reported elsewhere, was not observed with H_2 jets. However, such an effect cannot be excluded in a configuration promoting stronger interaction between both jets.
2. The H_2 jet ignites after a period of interaction with the burnt products from the pilot fuel. The duration of this interaction depends on the dwell time between the pilot SOI, the onset of jet interaction, and the charge temperature. A prolonged interaction is required for successful ignition under less reactive conditions and when the dwell time causes the pilot-fuel combustion products to lean-out and cool-down before the interaction begins.
3. The AHRR is dominated by the H_2 combustion and shows analogous characteristics to autoigniting diesel jets. The peak AHRR directly succeeds the ignition of the H_2 jet, and the peak AHRR amplitude increases with the elapsed time between H_2 SOI and ignition (*i.e.*, the mass of hydrogen within the jet at ignition). After the peak AHRR, a steady AHRR period with diffusion flame is established until the H_2 EOI. In most cases, the peak AHRR corresponds to the H_2 flame propagation from the ignition location across the H_2 jet volume.
4. When pilot-fuel ignites after the H_2 EOI, the jet-jet interaction occurs in H_2 jet region with a very lean H_2 equivalence ratio. This results in slower combustion propagation through the H_2 jet with large unburnt zones persisting late after ignition and large cyclic AHRR variability.
5. Very long pilot ignition delays induce a cyclic variability in the ignition delay, the pilot-ignition location, and the location of H_2 jet ignition. This cyclic variability results in variable flame evolution through the H_2 jet and associated AHRR variability.

Declaration of competing interest

The authors declare that they have no known competing financial interests or personal relationships that could have appeared to influence the work reported in this paper.

Acknowledgements

The financial support by the Australian Renewable Energy Agency (ARENA) and MAN Energy Solutions is gratefully appreciated. The first author acknowledges the support of the Commonwealth through the Australian Government Research Training Program Scholarship. The technical support during commissioning and operation of the CVCC facility by Mr Bryce Edmonds is also gratefully appreciated. The authors also acknowledge fruitful discussions with Dr Alexander Knafl and Marcus Becher from MAN Energy Solutions.

This Article has been authored by National Technology and Engineering Solutions of Sandia, LLC. under contract No. DE-NA0003525 with the U.S. Department of Energy/National Nuclear Security Administration. The United States Government retains and Elsevier, by accepting the article for publication, acknowledges that the United States Government retains a non-exclusive, paid-up, irrevocable, world-wide license to publish or reproduce the published form of this manuscript, or allow others to do so, for United States Government purposes.

REFERENCES

[1] Yip HL, Srna A, Yuen ACY, Kook S, Taylor RA, Yeoh GH, Medwell PR, Chan QN. A review of hydrogen direct injection for internal combustion engines: towards carbon-free combustion. Appl Sci 2019;9:4842.
[2] Berry GD, Pasternak AD, Rambach GD, Ray Smith J, Schock RN. Hydrogen as a future transportation fuel. Energy 1996;21:289–303.
[3] A review of hydrogen usage in internal combustion engines (gasoline-lpg-diesel) from combustion performance aspect. Int J Hydrogen Energy 2020;45:35257–68. 4th International HYDROGEN TECHNOLOGIES Congress.
[4] Verhelst S, Wallner T. Hydrogen-fueled internal combustion engines. Prog Energy Combust Sci 2009;35:490–527.
[5] Konnov AA, Mohammad A, Kishore VR, Kim NI, Prathap C, Kumar S. A comprehensive review of measurements and data analysis of laminar burning velocities for various fuel+air mixtures. Prog Energy Combust Sci 2018;68:197–267.
[6] Rosati MF, Aleiferis PG. Hydrogen SI and HCCI combustion in a direct-injection optical engine. SAE International Journal of Engines 2009;2:1710–36.
[7] Kawahara N, Tomita E. Visualization of auto-ignition and pressure wave during knocking in a hydrogen spark-ignition engine. Int J Hydrogen Energy 2009;34:3156–63.
[8] Liu X, Srna A, Yip HL, Kook S, Nian Q, Hawkes E. Comparison of hydrogen port injection and direct injection (DI) in a single-cylinder dual-fuel diesel engine. In: 22nd Australian fluid mechanics conference, AFMC2020. Brisbane, Australia: The University of Queensland; 2020.
[9] Lee K, Kim Y, Byun C, Lee J. Feasibility of compression ignition for hydrogen fueled engine with neat hydrogen-air pre-mixture by using high compression. Int J Hydrogen Energy 2013;38:255–64.
[10] Gomes Antunes J, Mikalsen R, Roskilly A. An experimental study of a direct injection compression ignition hydrogen engine. Int J Hydrogen Energy 2009;34:6516–22.
[11] White C, Steeper R, Lutz A. The hydrogen-fueled internal combustion engine: a technical review. Int J Hydrogen Energy 2006;31:1292–305.
[12] Zhai G, Xing S, Yuen AC, Medwell PR, Kook S, Yeoh GH, Chan QN. Laser ignition of iso-octane and n-heptane jets under compression-ignition conditions. Fuel 2021:122555.
[13] Van Blarigan P, Keller J. A hydrogen fuelled internal combustion engine designed for single speed/power operation. Int J Hydrogen Energy 1998;23:603–9.
[14] Homan H, Reynolds R, De Boer P, McLean W. Hydrogen-fueled diesel engine without timed ignition. Int J Hydrogen Energy 1979;4:315–25.
[15] Furuhama S, Kobayashi Y. Development of a hot-surface-ignition hydrogen injection two-stroke engine. Int J Hydrogen Energy 1984;9:205–13.
[16] Dimitriou P, Tsujimura T. A review of hydrogen as a compression ignition engine fuel. Int J Hydrogen Energy 2017;42:24470–86.
[17] Kumar M, Bhowmik S, Paul A. Effect of pilot fuel injection pressure and injection timing on combustion, performance and emission of hydrogen-biodiesel dual fuel engine. Int J Hydrogen Energy 2022;47:29554–67.
[18] Bakar R, Widudo, Kadirgama K, Ramasamy D, Yusaf T, Kamarulzaman M, Sivaraos, Aslfattahi N, Samylingam L, Alwayzy SH. Experimental analysis on the performance, combustion/emission characteristics of a di diesel engine using hydrogen in dual fuel mode. Int J Hydrogen Energy 2022.
[19] Woodyard D. Chapter two - dual-fuel and gas engines. In: Woodyard D, editor. Pounder's marine diesel engines and gas turbines. 9th ed. Oxford: Butterworth-Heinemann; 2009. p. 41–60.
[20] Liu H, Li J, Wang J, Wu C, Liu B, Dong J, Liu T, Ye Y, Wang H, Yao M. Effects of injection strategies on low-speed marine engines using the dual fuel of high-pressure direct-injection natural gas and diesel. Energy Sci Eng 2019;7:1994–2010.
[21] Li G. Optimization study of pilot-ignited natural gas direct-injection in diesel engines. SAE Trans 1999;108:1739–48.
[22] Liu J, Yang F, Wang H, Ouyang M, Hao S. Effects of pilot fuel quantity on the emissions characteristics of a CNG/diesel dual fuel engine with optimized pilot injection timing. Appl Energy 2013;110:201–6.
[23] Liu X, Srna A, Yip HL, Kook S, Chan QN, Hawkes ER. Performance and emissions of hydrogen-diesel dual direct injection (H2DDI) in a single-cylinder compression-ignition engine. Int J Hydrogen Energy 2021;46:1302–14.
[24] Y. Wang, A. Evans, A. Srna, A. Wehrfritz, E. Hawkes, X. Liu, S. Kook, Q. N. Chan, A numerical investigation of mixture formation and combustion characteristics of a hydrogen-diesel dual direct injection engine, SAE Paper 2021-01-0526 (2021).
[25] White TR. Simultaneous diesel and natural gas injection for dual-fuelling compression-ignition engines. Sydney, Australia: Ph.D. thesis, University of New South Wales; 2006.
[26] Fink G, Jud M, Sattelmayer T. Influence of the spatial and temporal interaction between diesel pilot and directly injected natural gas jet on ignition and combustion characteristics. J Eng Gas Turbines Power 2018;140:102811.
[27] Fink G, Jud M, Sattelmayer T. Fundamental study of diesel-piloted natural gas direct injection under different operating conditions. J Eng Gas Turbines Power 2019;141:091006.
[28] Yang X, Vinhaes VB, Turcios M, McTaggart-Cowan G, Huang J, Naber J, Shahbakhti M, Schmidt H, Atkinson W. Process for study of micro-pilot diesel-NG dual fuel combustion in a constant volume combustion vessel utilizing the premixed pre-burn procedure. 2019. SAE Paper 2019-01-1160.
[29] Trusca B. High pressure direct injection of natural gas and hydrogen fuel in a diesel engine. Ph.D. thesis. Canada: University of British Columbia; 2001.
[30] Ishibashi R, Tsuru D. An optical investigation of combustion process of a direct high-pressure injection of natural gas. J Mar Sci Technol 2017;22:447–58.
[31] Zhai G, Xing S, Yuen A, Yeoh GH, Chan QN. Spray and combustion characteristics of gasoline-like fuel under compression-ignition conditions. Energy Fuels 2020;34:16585–98.
[32] Xing S, Zhai G, Mo H, Medwell PR, Yuen AC, Kook S, Yeoh GH, Chan QN. Study of ignition and combustion characteristics of consecutive injections with iso-Octane and n-Heptane as fuels. Energy Fuels 2020;34:14741–56.
[33] Fattah IMR, Ming C, Chan QN, Wehrfritz A, Pham PX, Yang W, Kook S, Medwell PR, Yeoh GH, Hawkes ER, Masri AR. Spray and combustion investigation of post injections under low-temperature combustion conditions with biodiesel. Energy Fuels 2018;32:8727–42.
[34] Yip HL, Srna A, Liu X, Kook S, Hawkes ER, Chan QN. Visualization of hydrogen jet evolution and combustion under simulated direct-injection compression-ignition engine conditions. Int J Hydrogen Energy 2020;45:32562–78.
[35] Dec JE. A conceptual model of Dl diesel combustion based on laser-sheet imaging. SAE Trans 1997;106:1319–48.
[36] Woo C, Kook S, Rogers P, Marquis C, Hawkes E, Tupufia S. A comparative analysis on engine performance of a conventional diesel fuel and 10% biodiesel blends produced from coconut oils. SAE International Journal of Fuels and Lubricants 2015;8:597–609.

Please cite this article as: Rorimpandey P et al., Hydrogen-diesel dual-fuel direct-injection (H2DDI) combustion under compression-ignition engine conditions, International Journal of Hydrogen Energy, https://doi.org/10.1016/j.ijhydene.2022.09.241

[37] PubChem compound summary for CID 8900, heptane. 2022. . [Accessed 7 September 2022].
[38] Heywood J. Internal combustion engine fundamentals 2E. McGraw-Hill Education; 2018.
[39] Pickett LM, Kook S, Williams TC. Visualization of diesel spray penetration, cool-flame, ignition, high-temperature combustion, and soot formation Using high-speed imaging. SAE International Journal of Engines 2009;2:439–59.
[40] Liang X, Zhong A, Sun Z, Han D. Autoignition of n-heptane and butanol isomers blends in a constant volume combustion chamber. Fuel 2019;254:115638.
[41] Musculus MP, Miles PC, Pickett LM. Conceptual models for partially premixed low-temperature diesel combustion. Prog Energy Combust Sci 2013;39:246–83.
[42] Musculus M, Kattke K. Entrainment waves in diesel jets. SAE International Journal of Engines 2009;2:1170–93.
[43] Reitz R, Hessel R, Musculus M. A visual investigation of CFD-predicted in-cylinder mechanisms that control first- and second-stage ignition in diesel jets. 2019. SAE Paper 2019-01-0543.
[44] Knox BW, Genzale CL, Pickett LM, Garcia-Oliver JM, Vera-Tudela W. Combustion recession after end of injection in diesel sprays. SAE International Journal of Engines 2015;8:679–95.
[45] Zhai G, Xing S, Srna A, Wehrfritz A, Kook S, Hawkes ER, Chan QN. Ignition and flame stabilisation of primary reference fuel sprays at engine-relevant conditions. Combust Flame 2021;233:111620.
[46] Skeen S, Manin J, Pickett LM. Visualization of ignition processes in high-pressure sprays with multiple injections of n-Dodecane. SAE International Journal of Engines 2015;8:696–715.
[47] Zhang Y, Ito T, Nishida K. Characterization of mixture formation in split-injection diesel sprays via laser absorption-scattering (LAS) technique. SAE Trans 2001;110:2189–200.
[48] Anders JW, Magi V, Abraham J. A computational investigation of the interaction of pulses in two-pulse jets. Numer Heat Tran, Part A: Applications 2008;54:999–1021.
[49] Kook S, Pickett LM, Musculus MP. Influence of diesel injection parameters on end-of-injection liquid length recession. SAE International Journal of Engines 2009;2:1194–210.
[50] Network EC. Download code. 2019. https://ecn.sandia.gov/download-code/. [Accessed 14 February 2021].
[51] Pickett LM, Manin J, Genzale CL, Siebers DL, Musculus MP, Idicheria CA. Relationship between diesel fuel spray vapor penetration/dispersion and local fuel mixture fraction. SAE International Journal of Engines 2011;4:764–99.
[52] Shapiro ZM, Moffette TR. Hydrogen flammability data and application to pwr loss-of-coolant accident. 1957.
[53] Yip HL, Srna A, Wehrfritz A, Kook S, Hawkes ER, Chan QN. A parametric study of autoigniting hydrogen jets under compression-ignition engine conditions. Int J Hydrogen Energy 2022;47:21307–22.
[54] Liu X, Seberry G, Kook S, Chan QN, Hawkes ER. Direct injection of hydrogen main fuel and diesel pilot fuel in a retrofitted single-cylinder compression ignition engine. Int J Hydrogen Energy 2022.

Please cite this article as: Rorimpandey P et al., Hydrogen-diesel dual-fuel direct-injection (H2DDI) combustion under compression-ignition engine conditions, International Journal of Hydrogen Energy, https://doi.org/10.1016/j.ijhydene.2022.09.241